PERGAMON

International Journal of Solids and Structures 37 (2000) 6961–6980

INTERNATIONAL JOURNAL OF SOLIDS and STRUCTURES

www.elsevier.com/locate/ijsolstr

Refined semi-analytical design sensitivities

H. de Boer *, F. van Keulen

Koiter Institute Delft, Delft University of Technology, P.O. Box 5033, NL-2600 GA Delft, Netherlands

Received 12 October 1998

Abstract

Efficient structural optimization routines require availability of gradient information. Semi-analytical (SA) design sensitivities are rather popular, as they combine ease of implementation with computational efficiency. Their main drawback however, is their well-known inaccuracy problem for shape design sensitivities. It was found that the inaccuracies are especially unacceptable for slender structures and become more pronounced when relatively large rigid body motions can be identified for individual finite elements. Based on these observations, the authors recently developed a refined SA method taking full advantage of analytical differentiation of rigid body modes. The present article presents a sound and unified formulation of refined semi-analytical (RSA) design sensitivities for linear, linearized buckling, geometrically nonlinear and limit point analyses. Numerical results are presented in order to demonstrate the efficiency of the proposed method. It is concluded that the refined SA method possesses the advantages of the traditional SA method, whereas it does not exhibit its unacceptable inaccuracies.

Keywords: Design sensitivities; Semi-analytical; Buckling; Limit point

1. Introduction

Design and optimization processes may require accurate information on design sensitivities, i.e. information on the derivatives of response functions, such as stresses, strains and displacements, with respect to independent design variables. As the finite element (FE) method is nowadays a commonly used tool for analysing design alternatives, procedures for efficient and accurate evaluation of design sensitivities should complement existing FE packages.

In the literature, many approaches towards design sensitivity analysis can be found. The simplest among them is based on global finite difference (GFD) schemes. Implementation is easy and straightforward, but costs of computation can be high. Application of higher-order finite difference schemes is generally hindered by the computing costs involved. A further drawback is the required selection of design perturbations. Finally, the method's sensitivity to round-off errors is mentioned.

Design sensitivities on the basis of variational and analytical approaches do not suffer from the abovementioned drawbacks, i.e. computational efficiency is good and a selection of the design perturbation is not

* Corresponding author.

0020-7683/00/$ - see front matter
PII: S0020-7683(99)00322-4

needed. Typical examples can be found in Mróz and Haftka (1994) and Kleiber and Hien (1997). Formulation and implementation of these approaches are often involved.

As a compromise between global finite difference approaches and variational or analytical formulations, the so-called semi-analytical (SA) design sensitivities have been proposed; see Haftka and Adelman (1989) and the references given therein. Common feature of SA formulations is that their formulation starts analytically. In this way, design sensitivities are expressed in terms of (global) operators, e.g. the inverse of the tangent operator, and partial derivatives of quantities at the element level. In an SA formulation, the latter are replaced by finite difference approximations. This implies that design perturbations are still required. However, globally, the formulation benefits from an analytical approach, leading to computational efficient algorithms. Application of higher-order finite difference schemes at the element level requires, in contrast to GFD procedures, modest additional effort, both in terms of implementation and in terms of computing times. Implementation of SA design sensitivities in an existing FE code is easy. Often, the implementation can to a large extent be based on routines already available for structural analyses.

Early applications of SA design sensitivities indicated severe accuracy problems for shape design variables, see, e.g., Barthelemy et al. (1988) and Barthelemy and Haftka (1988). The accuracy of SA design sensitivities has been studied in the linear regime in a number of papers (Barthelemy and Haftka, 1988; Cheng et al., 1989; Pedersen et al., 1989; Fenyes and Lust, 1991; Olhoff and Rasmussen, 1991). These studies revealed that inaccuracies become more pronounced for slender structures and when FE meshes are refined. Depending on mesh density, slenderness of the structure and actual deformation pattern, the range of design perturbations leading to accurate design sensitivities may become small. Therefore, selection of design perturbation may become difficult and not suited for automated procedures. It was concluded, that the observed complications are associated with both the finite differences used at element level and the rigid body *rotations* of the individual elements, see Barthelemy et al. (1988) and Cheng and Olhoff (1993).

A number of improvements have been proposed in order to achieve accurate SA design sensitivities for a large range of design perturbations. In Barthelemy and Haftka (1988), Cheng et al. (1989) and Olhoff and Rasmussen (1991) application of higher-order finite difference schemes has been studied. Although a better accuracy is obtained, the source of the accuracy problems has not been removed, but the accuracy problem has been alleviated. This can be demonstrated easily using the beam example studied in Barthelemy et al. (1988), Barthelemy and Haftka (1988), Pedersen et al. (1989), Olhoff and Rasmussen (1991) and De Boer and Van Keulen (1997a). Following De Boer and Van Keulen (1997a), but using higher-order finite difference schemes, it follows that a strong dependence on the number of elements can still be observed. Thus, an application of higher-order finite difference schemes does not provide a rigorous solution to the accuracy problems observed.

Mlejnek (1992) explored the "natural approach" (Argyris and Mlejnek, 1986) to conserve consistency conditions for the rigid body rotations within the applied finite difference scheme. The method has been described for linear structural analyses. A combination with arbitrary finite difference schemes has not been addressed.

The so-called "exact" semi-analytical formulation (Olhoff et al., 1993) leads to exact derivatives. The method relies on specific features of the governing element matrices. "Exact" SA formulations have been applied for linear statics (Olhoff et al., 1993; Hinton et al., 1995), linearized buckling and free vibrations (Lund and Olhoff, 1994).

For linear structural analyses, the authors (Van Keulen and De Boer, 1998a) have proposed refined semi-analytical (RSA) design sensitivities. The underlying idea is to identify the rigid body modes of individual finite elements. These rigid body modes can be easily differentiated analytically with respect to the design variables. Consequently, the RSA formulation combines analytical derivatives with finite differences. In this way, the severe inaccuracies can be eliminated rigorously. This method has been studied analytically on the basis of the well-known beam example in De Boer and Van Keulen (1997a). This study revealed that results for the beam example are independent of the mesh density. Several advantages of the RSA method

can be mentioned. Firstly, it is easy to implement. Secondly, associated computational efforts are limited and, finally, the RSA method can be combined straightforwardly with arbitrary finite difference schemes.

Extension of the RSA formulation to linearized buckling has been discussed in Van Keulen and De Boer (1998b). Both numerical and analytical results have been presented, showing rigorous improvement of the accuracy. In De Boer and Van Keulen (1997b), a first attempt has been made to apply the RSA concept to geometrically nonlinear problems. The formulation lacks soundness as it has been formulated analogous to the linear formulation (Van Keulen and De Boer, 1998a).

The objective of the present article is to present RSA design sensitivities for a variety of structural analyses in a *unified* and *sound* formulation. Its application will be focused on geometrically nonlinear, limit point, linear and linearized buckling analyses. Apart from the formulation, aspects of implementation will be highlighted. The benefits of the RSA approach will be studied on the basis of a number of examples.

The layout of the present article is as follows: In Section 2, governing FE equations are discussed. In addition, rigid body motions and some of their properties will be reviewed. Special attention will be given to consistency conditions related to the rigid body modes and their partial derivatives. Section 3 addresses both SA and RSA design sensitivities for nonlinear, limit point, linear and linearized buckling analyses. Aspects of implementation are discussed in Section 4. Numerical examples are presented in Section 5. All numerical examples involve thin-walled structures and are modelled using the shell element reported in Van Keulen and Booij (1996). A final discussion and conclusions are subject of Section 6.

Throughout the present article, matrices will be denoted using bold capitals, e.g. $\mathbf{A}$. Vectors and one-dimensional arrays are referred to by bold lower-case characters, e.g. $\mathbf{a}$. It will be necessary to distinguish between quantities at system level and those corresponding to individual elements. This will be achieved by a superscript e for quantities corresponding to a single element. As an example, $\mathbf{u}$ refers to all nodal degrees of freedom, whereas $\mathbf{u}^e$ denotes the nodal degrees of freedom of a particular element. A partial derivative with respect to an arbitrary variable b, will be denoted $\ldots_{,b}$. Total derivatives are expressed as $d\ldots/db$.

The proposed RSA design sensitivities are applicable to every possible set of independent design variables $\mathbf{s}$. In order to simplify formulation and notation, focus will be on an arbitrary element s from the set $\mathbf{s}$. It is emphasized, that this does not impose any restriction on the formulation.

2. Preliminaries

In the present section, relevant FE characteristics are considered. In Section 2.1, the governing FE equations will be summarized. Rigid body modes corresponding to individual finite elements are reviewed in Section 2.2.

2.1. Governing finite element equations

At the element level, generalized deformations $\boldsymbol{\epsilon}^e$ can be expressed as functions of the nodal degrees of freedom $\mathbf{u}^e$ and a set of design variables $\mathbf{s}$. Thus,

$$\boldsymbol{\epsilon}^e = \boldsymbol{\epsilon}^e(\mathbf{u}^e; \mathbf{s}). \tag{1}$$

The generalized deformations are typically nonlinear in terms of both nodal degrees of freedom and design variables. It is important to emphasize that nodal degrees of freedom are implicit functions of design variables. In order to maintain a compact formulation, this implicit dependence is not expressed in the formulae.

Generalized stresses, energetically conjugated to $\boldsymbol{\epsilon}^e$, will be denoted $\boldsymbol{\sigma}^e$. In the case of linear elasticity, generalized stresses are determined by

$$\boldsymbol{\sigma}^e = \mathbf{D}^e(\mathbf{s})\boldsymbol{\epsilon}^e. \tag{2}$$

The matrix $\mathbf{D}^e$ depends on the material properties, the design variables and the actual element at hand.

With Eq. (1), the virtual work of deformation reads

$$\delta W_{\text{int}} = \sum \delta W^e_{\text{int}} = \sum \boldsymbol{\sigma}^{e\text{T}}\ \delta\boldsymbol{\epsilon}^e = \sum \boldsymbol{\sigma}^{e\text{T}}\ \mathbf{B}^e\ \delta\mathbf{u}^e = \mathbf{f}^{\text{T}}\ \delta\mathbf{u}, \tag{3}$$

where $\mathbf{B}^e$ is defined as

$$\mathbf{B}^e(\mathbf{u}^e;\mathbf{s}) = \boldsymbol{\epsilon}^e_{,\mathbf{u}^e}. \tag{4}$$

Notice that evaluation of δW_{int} requires volume integrations for the individual elements. These integrations have been entirely incorporated by proper and consistent definitions of the generalized stresses and deformations and the corresponding $\mathbf{D}^e$ and $\mathbf{B}^e$ matrices.

The load following from the discretized equations of equilibrium and the generalized stresses is denoted $\mathbf{f}(\mathbf{u};\mathbf{s})$. $\mathbf{f}$ is often referred to as the "internal load vector" and is evaluated on the basis of the individual element contributions

$$\mathbf{f}^e = \mathbf{B}^{e\text{T}}\boldsymbol{\sigma}^e. \tag{5}$$

The applied load will be denoted $\mathbf{p}$ and may depend on both nodal degrees of freedom and design variables. Moreover, it is often convenient to scale the applied load with a load parameter λ. The corresponding virtual work reads

$$\delta W_{\text{ext}} = \mathbf{p}(\lambda;\mathbf{u};\mathbf{s})^{\text{T}}\delta\mathbf{u}. \tag{6}$$

With the principle of virtual work, it follows from Eqs. (3) and (6) that

$$\mathbf{f}(\mathbf{u};\mathbf{s}) = \mathbf{p}(\lambda;\mathbf{u};\mathbf{s}), \tag{7}$$

which are the well-known equations of equilibrium.

After the introduction of a monotonously increasing quantity τ, which could be identified as a control variable (Riks, 1997), rate equations follow from (2)–(7) as

$$\mathbf{J}\frac{\mathrm{d}\mathbf{u}}{\mathrm{d}\tau} = \mathbf{p}_{,\lambda}\frac{\mathrm{d}\lambda}{\mathrm{d}\tau}. \tag{8}$$

The Jacobian $\mathbf{J}$ is assembled from individual element contributions $\mathbf{J}^e$, which are given by

$$\mathbf{J}^e = \mathbf{K}^e + \mathbf{G}^e - \mathbf{p}^e_{,\mathbf{u}^e}. \tag{9}$$

Here $\mathbf{K}^e$ and $\mathbf{G}^e$ are given by

$$\mathbf{K}^e = \mathbf{B}^{e\text{T}}\mathbf{D}^e\mathbf{B}^e, \tag{10}$$

$$\mathbf{G}^e = \boldsymbol{\sigma}^{e\text{T}}\mathbf{B}^e_{,\mathbf{u}^e} \tag{11}$$

and refer to the physical and geometrical stiffness, respectively.

2.2. Rigid body modes

For the present article, it is essential to define for each element a basis for *all* possible rigid body modes. In the *actual configuration*, a rigid body mode $\boldsymbol{\rho}^e$ is characterized by the fact that the corresponding deformation rates are zero. With Eqs. (1) and (4) this can be formulated as

$$\mathbf{B}^e\boldsymbol{\rho}^e = \mathbf{0}. \tag{12}$$

It is emphasized that $\mathbf{B}^e$ is a function of the nodal degrees of freedom and the rigid body modes are defined for the actual configuration. Provided no spurious energy modes are available, the space of rigid body modes corresponds to the *kernel* of the linear mapping represented by $\mathbf{B}^e$. At this point, an orthogonal basis $\{\mathbf{r}_k^e(\mathbf{u}^e;\mathbf{s})\}$ is introduced for the kernel of this mapping. Index k ranges from one to the number of independent rigid body modes to be described by the element under consideration.

As the basis vectors $\mathbf{r}_k^e$ satisfy Eq. (12) for *any* configuration $(\mathbf{u}^e;\mathbf{s})$, differentiation of $\mathbf{B}^e\mathbf{r}_k^e = \mathbf{0}$ with respect to $\mathbf{u}^e$ leads to a first consistency condition

$$(\mathbf{B}^e\mathbf{r}_k^e)_{,\mathbf{u}^e} = \mathbf{0}. \tag{13}$$

Similarly, differentiation with respect to the design variable s yields

$$(\mathbf{B}^e\mathbf{r}_k^e)_{,\mathbf{u}^e}\frac{\mathrm{d}\mathbf{u}^e}{\mathrm{d}s} + (\mathbf{B}^e\mathbf{r}_k^e)_{,s} = \mathbf{0}. \tag{14}$$

By combining Eqs. (13) and (14), it follows

$$\mathbf{B}^e_{,s}\mathbf{r}_k^e + \mathbf{B}^e\mathbf{r}_{k,s}^e = \mathbf{0}, \tag{15}$$

which provides a second consistency equation for the basis vectors $\mathbf{r}_k^e$.

For the present article, a more careful inspection of the second consistency equation is of crucial importance. Partial derivatives of $\mathbf{B}^e$ can be evaluated analytically, but their derivation and implementation can be tedious. In contrast to this observation, partial derivatives of $\mathbf{r}_k^e$ can easily be evaluated analytically. Moreover, these derivatives can be evaluated without information on the precise formulation of the element at hand. More details on construction of the basis $\{\mathbf{r}_k^e\}$ and corresponding derivatives will be given in Section 4.

The basis vectors $\mathbf{r}_k^e$ will be used in two ways: Firstly, they are used to decompose arbitrary nodal velocities into a deformational and a rigid body component. To be more precise, for linear analyses, the nodal displacements and the nodal rotations will be decomposed. For linearized buckling analyses the buckling modes will be decomposed at the element level. A similar approach will be followed for limit point analyses, whereas it seems not applicable to nonlinear analyses. Secondly, the basis vectors will be invoked to decompose pseudo-loads into a self-equilibrating component and one which is not. For these purposes, it is convenient to introduce a matrix $\mathbf{S}^e$, which is defined as

$$\mathbf{S}^e = \sum_k \frac{\mathbf{r}_k^e\mathbf{r}_k^{e\mathrm{T}}}{\mathbf{r}_k^{e\mathrm{T}}\mathbf{r}_k^e}. \tag{16}$$

Assuming nodal velocities $\mathbf{v}^e$, the component of $\mathbf{v}^e$ along $\mathbf{r}_k^e$ is given by $(\mathbf{r}_k^{e\mathrm{T}}\mathbf{r}_k^e)^{-1}(\mathbf{r}_k^{e\mathrm{T}}\mathbf{v}^e)\mathbf{r}_k^e$, where $(\mathbf{r}_k^{e\mathrm{T}}\mathbf{r}_k^e)^{-1}$ accounts for the fact that the basis vectors $\mathbf{r}_k^e$ are mutually orthogonal, but nonnormalized. Consequently, the entire rigid body component contained by $\mathbf{v}^e$ follows as $\mathbf{S}^e\mathbf{v}^e$. If $\mathbf{q}^e$ refers to an arbitrary load acting on an element, then $\mathbf{S}^e\mathbf{q}^e$ represents the load component which is not self-equilibrating. This is seen from the fact that $\mathbf{q}^e - \mathbf{S}^e\mathbf{q}^e$ represents the self-equilibrating component of $\mathbf{q}^e$. The latter observation can be proven using the principle of virtual work together with a virtual displacement field containing rigid body modes only and the fact that $\mathbf{r}_k^{e\mathrm{T}}(\mathbf{q}^e - \mathbf{S}^e\mathbf{q}^e) = 0$. In addition to $\mathbf{S}^e$, a matrix $\mathbf{F}^e$ is introduced as

$$\mathbf{F}^e = \mathbf{I} - \mathbf{S}^e. \tag{17}$$

This matrix can be used in a similar manner as $\mathbf{S}^e$ to extract the deformational velocity component or the self-equilibrating load component, respectively. Note that both $\mathbf{S}^e$ and $\mathbf{F}^e$ are symmetric.

The partial derivatives of $\mathbf{F}^e$ and $\mathbf{S}^e$ with respect to a design variable s are given by

$$\mathbf{F}^e_{,s} = -\mathbf{S}^e_{,s} = \mathring{\mathrm{F}}^e + \mathring{\mathrm{F}}^{e\mathrm{T}} + 2\sum(\mathbf{r}_{k,s}^{e\mathrm{T}}\mathbf{r}_k^e)\frac{\mathbf{r}_k^e\mathbf{r}_k^{e\mathrm{T}}}{(\mathbf{r}_k^{e\mathrm{T}}\mathbf{r}_k^e)^2}. \tag{18}$$

Here $\mathring{\mathbf{F}}^e$ refers to a *pseudo-gradient*, which is defined as

$$\mathring{\mathbf{F}}^e = -\sum_k \frac{\mathbf{r}^e_{k,s}\mathbf{r}^{e\mathrm{T}}_k}{\mathbf{r}^{e\mathrm{T}}_k\mathbf{r}^e_k}. \tag{19}$$

Note that $\mathring{\mathbf{F}}^e$ is non-symmetric. With the definitions (16) and (19) and consistency equation (15), it is easy to verify that

$$\mathbf{B}^e_{,s}\mathbf{S}^e = \mathbf{B}^e\mathring{\mathbf{F}}^e. \tag{20}$$

This consistency equation will be used frequently to replace partial derivatives of $\mathbf{B}^e$ by partial derivatives of $\mathbf{r}^e_k$.

3. Design sensitivities

In order to achieve a general starting point, it is assumed that the load parameter λ can be a function of the design variables. In this case, a straightforward differentiation of the equations of equilibrium (7) with respect to s yields

$$\mathbf{J}\frac{\mathrm{d}\mathbf{u}}{\mathrm{d}s} - \mathbf{p}_{,\lambda}\frac{\mathrm{d}\lambda}{\mathrm{d}s} = \mathbf{p}_{,s} - \mathbf{f}_{,s}. \tag{21}$$

Here, use has been made of the fact that $\mathbf{f}_{,\mathbf{u}} - \mathbf{p}_{,\mathbf{u}} = \mathbf{J}$, where $\mathbf{J}$ denotes the Jacobian, see also Eqs. (8) and (9).

The above result will be the starting point for the discussion of both SA and RSA design sensitivities. Design sensitivities in case of geometrical non-linearities are considered in Section 3.1. Limit loads are dealt with in Section 3.2. The linear equivalents of Sections 3.1 and 3.2 are given in Sections 3.3 and 3.4, respectively.

3.1. Geometrically nonlinear analysis

When the load parameter is independent of the design variables, Eq. (21) reduces to

$$\mathbf{J}\frac{\mathrm{d}\mathbf{u}}{\mathrm{d}s} = \mathbf{p}_{,s} - \mathbf{f}_{,s}. \tag{22}$$

This result is well known and can also be found in Haftka (1993), among others. The term $\mathbf{p}_{,s} - \mathbf{f}_{,s}$ is often referred to as the *pseudo-load*. Displacement sensitivities for geometrically nonlinear responses follow directly from Eq. (22) as

$$\frac{\mathrm{d}\mathbf{u}}{\mathrm{d}s} = \mathbf{J}^{-1}(\mathbf{p}_{,s} - \mathbf{f}_{,s}). \tag{23}$$

Here, regularity of the Jacobian matrix $\mathbf{J}$ is assumed, which implies that Eq. (23) is not applicable to stability points.

In a traditional SA method, partial derivatives in Eq. (23) are evaluated on the basis of finite differences. Notice that $\mathbf{f}_{,s}$ can be obtained by applying finite difference approximations either at the system or the element level. If evaluated at the element level, corresponding contributions become

$$\mathbf{f}^e_{,s} = \mathbf{B}^{e\mathrm{T}}_{,s}\boldsymbol{\sigma}^e + \mathbf{B}^{e\mathrm{T}}\boldsymbol{\sigma}^e_{,s}, \tag{24}$$

which follows from Eq. (5). As mentioned in Section 1, it was found for linear problems that severe inaccuracies of SA shape design sensitivities originate from replacing $\mathbf{f}^e_{,s}$ by its finite difference approximation.

These inaccuracies are strongly influenced by the design perturbation Δs used to evaluate the finite difference approximations. Similar approximations applied to $\mathbf{p}_{,s}$ did not give rise to accuracy problems. Further, it was shown that inaccuracies may become severe if the components representing the rigid body rotations contained in the vector of nodal degrees of freedom are large as compared to the corresponding deformation component.

To achieve more accurate SA design sensitivities, the right hand side of Eq. (24) is inspected more precisely. The first term gives a contribution which might not be self-equilibrating. The second term, however, yields a self-equilibrating contribution to the pseudo-load, as $\mathbf{r}_k^{e\mathrm{T}}\mathbf{B}^{e\mathrm{T}}\boldsymbol{\sigma}_{,s}^e = \mathbf{0}$ for all possible k. Referring to Saint–Venant's principle, it should be expected that errors introduced by the finite difference approximations to $\boldsymbol{\sigma}_{,s}^e$ tend to damp out. This in contrast to errors introduced by finite difference approximations to $\mathbf{B}_{,s}^e$. Therefore, $\mathbf{B}_{,s}^{e\mathrm{T}}\boldsymbol{\sigma}^e$ will be decomposed into a self-equilibrating component and one which is not. Thus, with reference to Eq. (16) and using Eq. (17), Eq. (24) becomes

$$\mathbf{f}_{,s}^e = \mathbf{S}^e\mathbf{B}_{,s}^{e\mathrm{T}}\boldsymbol{\sigma}^e + \mathbf{F}^e\mathbf{B}_{,s}^{e\mathrm{T}}\boldsymbol{\sigma}^e + \mathbf{B}^{e\mathrm{T}}\boldsymbol{\sigma}_{,s}^e. \tag{25}$$

Examining this result, it is seen that only the first term in the right hand side gives a contribution which is not self-equilibrating. Applying consistency condition Eq. (20), this term can be replaced by one which only involves partial derivatives of $\mathbf{r}_k^e$:

$$\mathbf{f}_{,s}^e = \mathring{\mathrm{F}}^{e\mathrm{T}}\mathbf{B}^{e\mathrm{T}}\boldsymbol{\sigma}^e + \mathbf{F}^e\mathbf{B}_{,s}^{e\mathrm{T}}\boldsymbol{\sigma}^e + \mathbf{B}^{e\mathrm{T}}\boldsymbol{\sigma}_{,s}^e. \tag{26}$$

In the RSA formulation, partial derivatives of $\boldsymbol{\sigma}^e$ and $\mathbf{B}^e$ are evaluated using finite difference approximations at element level. Components of $\mathring{\mathrm{F}}^e$ are computed by taking full advantage of analytical derivatives $\mathbf{r}_{k,s}^e$. Consequently, errors introduced by the finite difference approximations are of a self-equilibrating nature and their effect damps out.

For many purposes, strain and stress sensitivities are required. For that purpose Eq. (1) is differentiated with respect to s, leading to

$$\frac{\mathrm{d}\boldsymbol{\epsilon}^e}{\mathrm{d}s} = \mathbf{B}^e\frac{\mathrm{d}\mathbf{u}^e}{\mathrm{d}s} + \boldsymbol{\epsilon}_{,s}^e. \tag{27}$$

Using Eq. (2), the stress sensitivities become

$$\frac{\mathrm{d}\boldsymbol{\sigma}^e}{\mathrm{d}s} = \mathbf{D}_{,s}^e\boldsymbol{\epsilon}^e + \mathbf{D}^e\frac{\mathrm{d}\boldsymbol{\epsilon}^e}{\mathrm{d}s}. \tag{28}$$

Again, finite differences are applied to obtain $\boldsymbol{\epsilon}_{,s}^e$ and $\mathbf{D}_{,s}^e$, whereas $\mathrm{d}\mathbf{u}^e/\mathrm{d}s$ and $\mathrm{d}\boldsymbol{\epsilon}^e/\mathrm{d}s$ follow from Eqs. (23) and (27), respectively. The difference between SA and RSA strain sensitivities is that the RSA method evaluates $\mathrm{d}\mathbf{u}^e/\mathrm{d}s$ by using Eq. (26), whereas the traditional SA method uses $\Delta\mathbf{f}^e/\Delta s$.

3.2. Limit points

A stability point is characterized by a singular Jacobian matrix $\mathbf{J}$, see for more details Riks (1997) and references given therein. The singularity is also reflected by a zero eigenvalue for $\mathbf{J}$. In the sequel, it is assumed that the zero eigenvalue of $\mathbf{J}$ is distinct and complications related to multiple eigenvalues are not addressed here. Moreover, it is assumed that the Jacobian matrix is symmetric. A stability point $(\mathbf{u} = \mathbf{u}_c; \lambda = \lambda_c)$ can now be characterized by

$$\mathbf{J}_c\mathbf{v} = \mathbf{0}, \tag{29}$$

where $\mathbf{v}$ denotes the eigenvector associated with the zero eigenvalue. The subscript c indicates evaluation for $(\mathbf{u}_c; \lambda_c)$.

If it is now assumed, that λ is controlled in such a way that it always corresponds to $\lambda = \lambda_c$, then Eq. (21) can be written as

$$\mathbf{J}_c \frac{\mathrm{d}\mathbf{u}_c}{\mathrm{d}s} - (\mathbf{p}_{,\lambda})_c \frac{\mathrm{d}\lambda_c}{\mathrm{d}s} = (\mathbf{p}_{,s} - \mathbf{f}_{,s})_c. \tag{30}$$

It is often the case that the only design sensitivities that are relevant are those for λ_c. For that reason, Eq. (30) is pre-multiplied by $\mathbf{v}^{\mathrm{T}}$, which gives together with Eq. (29) (Wu and Arora, 1987, 1988; Haftka, 1993)

$$\frac{\mathrm{d}\lambda_c}{\mathrm{d}s} = -\frac{\mathbf{v}^{\mathrm{T}}(\mathbf{p}_{,s} - \mathbf{f}_{,s})_c}{\mathbf{v}^{\mathrm{T}}(\mathbf{p}_{,\lambda})_c}. \tag{31}$$

It is emphasized that Eq. (31) is not applicable to bifurcation points, as for a bifurcation point $\mathbf{v}^{\mathrm{T}}(\mathbf{p}_{,\lambda})_c$ becomes zero, see, e.g. Riks (1997).

In an SA formulation the terms $(\mathbf{p}_{,s})_c$ and $(\mathbf{f}_{,s})_c$ are approximated using finite differences, either at the system or the element level. Here, the focus will be on element level. In this case, $(\mathbf{f}^e_{,s})_c$ will be evaluated using a finite difference approximation to Eq. (24) for $(\mathbf{u}_c; \lambda_c)$. An RSA formulation is obtained if $(\mathbf{f}^e_{,s})_c$ is calculated on the basis of Eq. (26). In this way, the RSA formulation is based on a decomposition of $(\mathbf{f}^e_{,s})_c$ into a self-equilibrating component and one which is not. An alternative starting point for the RSA formulation is to decompose $\mathbf{v}^e$ into a deformational and a rigid body component. This approach, in combination with consistency condition Eq. (20), leads to exactly the same RSA formulation as obtained directly on the basis of Eq. (26).

3.3. Linear analysis

Linear problems are governed by the well-known relation $\mathbf{p}_0 = \mathbf{K}_0\mathbf{u}$. Here, a subscript 0 indicates evaluation for $\mathbf{u} = \mathbf{0}$. The design sensitivities for the nodal degrees of freedom follow as (Haftka and Adelman, 1989)

$$\frac{\mathrm{d}\mathbf{u}}{\mathrm{d}s} = \mathbf{K}_0^{-1}\left(\mathbf{p}_{0,s} - \mathbf{K}_{0,s}\mathbf{u}\right). \tag{32}$$

Notice that for any quantity $a(\mathbf{u}; \mathbf{s})$, it follows $\mathrm{d}a_0/\mathrm{d}s = a_{0,s}$. In an SA formulation, the derivatives $\mathbf{K}_{0,s}$ are approximated using finite differences.

As mentioned, severe inaccuracies were shown to originate from replacing $\mathbf{K}_{0,s}$ by its finite difference approximation. Focus will therefore be on $\mathbf{f}_{,s} = \mathbf{K}_{0,s}\mathbf{u}$, which will be assembled from individual element contributions $\mathbf{f}^e_{,s} = \mathbf{K}^e_{0,s}\mathbf{u}^e$. Before starting a refined formulation, it is noted that, analogous to consistency condition Eq. (20), the following consistency equation has to be satisfied

$$\mathbf{K}^e_{0,s}\mathbf{S}^e_0 = \mathbf{K}^e_0\mathring{\mathrm{F}}^e_0 \tag{33}$$

in the linear regime. This relation is easily verified using Eqs. (10), (12), (16) and (19). Similar to the RSA formulation for nonlinear analyses given in Section 3.1, the contribution $\mathbf{f}^e_{,s}$ is decomposed into a self-equilibrating component and one which is not. Together with consistency condition (33), this decomposition yields

$$\mathbf{f}^e_{,s} = \mathring{\mathrm{F}}^{e\mathrm{T}}_0\mathbf{K}^e_0\mathbf{u}^e + \mathbf{F}^e_0\mathbf{K}^e_{0,s}\mathbf{u}^e. \tag{34}$$

The first term in the right hand side of Eq. (34) can be evaluated analytically, provided analytical derivatives for rigid body modes are available. The second term in the right hand side of Eq. (34) is self-equilibrating. In the nonlinear formulation, the calculation of $\boldsymbol{\epsilon}^e_{,s}$ involves the calculation of the generalized deformations in the configuration $(\mathbf{u}^e; s + \Delta s)$. In the linear formulation, this is not done explicitly, as use is

made of a linearization in the configuration ($\mathbf{u}^e = \mathbf{0}$). This aspect is finally reflected by a somewhat different composition of the contribution to the pseudo-load vector, compare Eqs. (26) and (34). In the present case, however, the second term in the right hand side of Eq. (34) permits a further improvement. For this purpose, $\mathbf{u}^e$ is decomposed into a deformational and a rigid body component. In addition, this decomposition is simple in the linear regime, as $\mathbf{u}^e$ can be projected directly on $\mathbf{r}_k^e$, which is not permitted in the nonlinear regime involving finite rotations. With this decomposition, Eq. (17), consistency condition (33), and $\mathbf{K}_0^e\mathbf{S}_0^e = 0$ it follows

$$\mathbf{f}_{,s}^e = \mathring{\mathbf{F}}_0^{e\mathrm{T}}\mathbf{K}_0^e\mathbf{u}^e + \mathbf{K}_0^e\mathring{\mathbf{F}}_0^e\mathbf{u}^e + \mathbf{F}_0^e\mathbf{K}_{0,s}^e\mathbf{F}_0^e\mathbf{u}^e. \tag{35}$$

Both the first and second term can be evaluated accurately using analytical derivatives for the rigid body modes. In the RSA formulation, the last term in the right hand side of Eq. (35) will be approximated by means of finite differences. Note that the associated errors only depend on the deformational component of $\mathbf{u}^e$, rather than on $\mathbf{u}^e$. Moreover, the error contribution is self-equilibrating. Hence, referring to Saint-Venant's principle, the effects caused by the error contribution corresponding to a single element tends to damp out. This in contrast to a direct application of $\mathbf{K}_{0,s}^e\mathbf{u}^e$, for which the associated errors might spread over the entire domain of the finite element model used.

Once having obtained $\mathrm{d}\mathbf{u}/\mathrm{d}s$, design sensitivities for strains and stresses can be evaluated at element level. The generalized strains are determined from a linearization of Eq. (1)

$$\boldsymbol{\epsilon}^e = \mathbf{B}_0^e\mathbf{u}^e. \tag{36}$$

Consequently, strain sensitivities for linear analyses are determined by

$$\frac{\mathrm{d}\boldsymbol{\epsilon}^e}{\mathrm{d}s} = \mathbf{B}_0^e\frac{\mathrm{d}\mathbf{u}^e}{\mathrm{d}s} + \mathbf{B}_{0,s}^e\mathbf{u}^e. \tag{37}$$

In an SA formulation, $\mathbf{B}_{0,s}^e$ is approximated using finite differences. Corresponding stress sensitivities are evaluated using Eq. (28). RSA strain sensitivities start from a decomposition of $\mathbf{u}^e$. Thus, $\boldsymbol{\epsilon}^e = \mathbf{B}_0^e\mathbf{u}^e$ is replaced by $\boldsymbol{\epsilon}^e = \mathbf{B}_0^e\mathbf{F}_0^e\mathbf{u}^e$, which, by a straightforward differentiation and application of Eq. (18), leads to

$$\frac{\mathrm{d}\boldsymbol{\epsilon}^e}{\mathrm{d}s} = \mathbf{B}_0^e\frac{\mathrm{d}\mathbf{u}^e}{\mathrm{d}s} + \mathbf{B}_0^e\mathring{\mathbf{F}}_0^e\mathbf{u}^e + \mathbf{B}_{0,s}^e\mathbf{F}_0^e\mathbf{u}^e. \tag{38}$$

This expression is evaluated using finite difference approximations for the last term. Errors introduced by these approximations are now only multiplied by the deformational component of $\mathbf{u}^e$, this in contrast to Eq. (37) for which the errors are multiplied by $\mathbf{u}^e$.

The RSA formulation for linear structural analyses was first proposed in Van Keulen and De Boer (1998a) and studied analytically in De Boer and Van Keulen (1997a). The formulations given here and in Van Keulen and De Boer (1998a) are essentially the same. However, there are three important aspects that motivated the detailed discussion given above. Firstly, stress and strain sensitivities were not addressed in Van Keulen and De Boer (1998a). As these require more attention in an RSA formulation, they have been included here. A second, more fundamental, aspect is that the present formulation is entirely consistent with the approach followed for the nonlinear regime. For this reason, the starting point for the RSA formulation had to be selected differently. To be more precise, the present formulation started with a decomposition of the pseudo-load vector, whereas a decomposition of the nodal degrees of freedom was the starting point in Van Keulen and De Boer (1998a). Finally, in Van Keulen and De Boer (1998a) the decomposition of the pseudo-load vector into a self-equilibrating component and one which is not, was not apparent at all. Being aware of the consequences of this decomposition, results in a better understanding of the actual nature of the proposed refinements and the origin of the severe inaccuracies associated with SA design sensitivities.

3.4. Linearized buckling

In structural optimization, stability aspects are often of primary importance. For this reason and completeness of the present article, RSA design sensitivities for linearized buckling are summarized here. For more details and an analytical study, the reader is referred to Van Keulen and De Boer (1998b).

A linear pre-buckling solution is assumed. In this case, buckling analysis is governed by the eigenvalue problem

$$(\mathbf{K}_0 + \mu \mathbf{G}_0)\mathbf{v} = \mathbf{0}. \tag{39}$$

Here $\mathbf{G}_0$ is the geometrical stiffness corresponding to the pre-buckling solution. To reach a critical load level, the applied load must be scaled with the eigenvalue μ. The corresponding buckling mode is denoted by $\mathbf{v}$. It is assumed that the eigenvalues are distinct. For an overview of multiple eigenvalues in structural optimization problems, the reader is referred to Seyranian et al. (1994).

Design sensitivities for the eigenvalue μ follow by differentiation of Eq. (39) and pre-multiplying the result by $\mathbf{v}^{\mathrm{T}}$. This gives

$$\frac{\mathrm{d}\mu}{\mathrm{d}s} = -\frac{\mathbf{v}^{\mathrm{T}}\mathbf{K}_{0,s}\mathbf{v} + \mu\mathbf{v}^{\mathrm{T}}\mathbf{G}_{0,s}\mathbf{v}}{\mathbf{v}^{\mathrm{T}}\mathbf{G}_0\mathbf{v}}, \tag{40}$$

which can be found in Haftka and Gürdal (1992) and Lund and Olhoff (1994), among many others. In an SA formulation, both $\mathbf{K}_{0,s}$ and $\mathbf{G}_{0,s}$ are approximated using finite differences. Note that for evaluation of $\mathbf{G}_{0,s}$, stress sensitivities for the pre-buckling state are required.

The finite difference approximations to $\mathbf{v}^{\mathrm{T}}\mathbf{K}_{0,s}\mathbf{v}$ may lead to severe inaccuracies (Van Keulen and De Boer, 1998b). However, an improvement along the lines followed in previous sub-sections is possible. For this reason, the individual element contributions $\mathbf{v}^{e\mathrm{T}}\mathbf{K}^e_{0,s}\mathbf{v}^e$ are studied. Here a decomposition of the buckling mode at element level $\mathbf{v}^e$ into a rigid body and a deformational component is applied. For this purpose, the $\mathbf{S}^e_0$ and $\mathbf{F}^e_0$ matrices are used. These matrices are defined in Eqs. (16) and (17), respectively. Using this decomposition and consistency condition (33), $\mathbf{v}^{e\mathrm{T}}\mathbf{K}^e_{0,s}\mathbf{v}^e$ can be written as

$$\mathbf{v}^{e\mathrm{T}}\mathbf{K}^e_{0,s}\mathbf{v}^e = \mathbf{v}^{e\mathrm{T}}\left(2\mathring{\mathbf{F}}^{e\mathrm{T}}_0\mathbf{K}^e_0 + \mathbf{F}^e_0\mathbf{K}^e_{0,s}\mathbf{F}^e_0\right)\mathbf{v}^e. \tag{41}$$

In the RSA formulation, analytical derivatives are being used for $\mathring{\mathbf{F}}^e_0$, whereas $\mathbf{K}^e_{0,s}$ is approximated using finite differences. However, the latter contribution is only coupled with the deformational component of $\mathbf{v}^e$.

The derivatives of the geometrical stiffness are improved indirectly, as an RSA formulation is used for the pre-buckling solution and the associated pre-buckling stresses. An elegant RSA formulation for the entire contribution corresponding to $\mu\mathbf{v}^{e\mathrm{T}}\mathbf{G}^e_{0,s}\mathbf{v}^e$ is lacking. However, the analytical example studied in Van Keulen and De Boer (1998b) indicates that this term leads to less severe inaccuracies as compared to errors associated with $\mathbf{v}^{e\mathrm{T}}\mathbf{K}^e_{0,s}\mathbf{v}^e$.

4. Aspects of implementation

The objective of the present section is to illustrate that it is relatively simple to implement the RSA method in an existing FE package. The discussion will be focused on nonlinear and linear analyses only. The starting point will be the implementation of a framework for computing traditional SA design sensitivities. Once having implemented such a scheme, the following modifications must be applied:

- Evaluate finite difference approximations at the element level rather than at the system level. The reason is that consistency equation Eq. (20) can only be defined at the element level.
- Compute rigid body modes and corresponding derivatives for each element.

- Evaluate $\mathbf{f}^e_{,s}$ by applying Eqs. (26) or (35) instead of replacing it directly by its finite difference approximation.

As the modifications only involve some basic vector operations, the additional computing time turns out to be negligible.

The second item requires some elaboration. In Van Keulen and De Boer (1998a), it has been noted that implementation of rigid body modes and their derivatives can be realized for classes of finite elements, without knowing all the details of their specific formulation. Here, this aspect will be worked out in more detail. In contrast to Van Keulen and De Boer (1998a), the present discussion is not restricted to the linear case. It is mentioned, that implementation of the basis vectors and their derivatives does require changes for the nonlinear regime. The most important being the dependence of rigid body modes on nodal degrees of freedom.

It is assumed that the element under consideration resides in a space with three dimensions. The rigid body modes of a single element will be considered as a function of its location in space. For the time being, focus will be on an arbitrary material point of the element under consideration. The rigid body modes can be described by superposition of a translational and a rotational mode. Hence, the corresponding velocity field $\mathbf{q}^e$ becomes

$$\mathbf{q}^e = \mathbf{t}^e + \boldsymbol{\omega}^e \times (\mathbf{x}_0 + \hat{\mathbf{u}}^e). \tag{42}$$

Here $\mathbf{t}^e$ represents the velocity at the origin and $\boldsymbol{\omega}^e$ is a spin vector. Note that both $\mathbf{t}^e$ and $\boldsymbol{\omega}^e$ are arbitrary. The location in the undeformed configuration of the present material point is $\mathbf{x}_0$ and the corresponding displacement vector is $\hat{\mathbf{u}}^e$. The hat has been introduced to distinguish from nodal degrees of freedom $\mathbf{u}^e$. The location $\mathbf{x}_0$ is, in the case of shape design variables, an explicit function of design variables. As a rigid body motion of a single element is considered, the spin vector will be identical for all material points and equals $\boldsymbol{\omega}^e$.

A simple approach to construct six independent rigid body modes is to select all components of $\mathbf{t}^e$ and $\boldsymbol{\omega}^e$, but one, to be zero. In this way, the following six rigid body modes are constructed

$$\begin{aligned} &\mathbf{q}^e_i = \mathbf{e}_i, && \boldsymbol{\omega}^e_i = \mathbf{0}, && i = 1,2,3, \\ &\mathbf{q}^e_{i+3} = \mathbf{e}_i \times (\mathbf{x}_0 + \hat{\mathbf{u}}^e), && \boldsymbol{\omega}^e_{i+3} = \mathbf{e}_i, && i = 1,2,3. \end{aligned} \tag{43}$$

Here $\mathbf{e}_i$ refers to three orthonormal vectors.

These rigid body modes are the starting point for the generation of six rigid body modes, $\boldsymbol{\rho}^e_i$, $i = 1,\ldots,6$, in terms of nodal degrees of freedom. For this purpose, the precise definition of the nodal degrees of freedom is required. In general, components of $\boldsymbol{\rho}^e_i$ corresponding with nodal displacements can be derived using the velocity field $\mathbf{q}^e$. Components corresponding with nodal rotations can be obtained using the spin vector $\boldsymbol{\omega}^e$.

Following Van Keulen and De Boer (1998a), a classical Schmidt orthogonalization procedure will be applied to construct an orthogonal basis $\{\mathbf{r}^e_k\}$ from the modes $\boldsymbol{\rho}^e_i$. Of importance is the observation that it is most convenient to start the orthogonalization procedure with translational modes. The reason for this is that translational modes are already orthogonal and their design sensitivities equal zero. The orthogonalization finally yields

$$\mathbf{r}^e_k = \sum_{i=1}^{6} a^e_{ki} \boldsymbol{\rho}^e_i, \tag{44}$$

with a^e_{ki} being the components of $\mathbf{r}^e_k$ with respect to $\boldsymbol{\rho}^e_i$, which have been determined by the Schmidt orthogonalization. Derivatives of rigid body modes now become

$$\mathbf{r}^e_{k,s} = \sum_{i=1}^{6} a^e_{ki}\boldsymbol{\rho}^e_{i,s} + \sum_{i=1}^{6} a^e_{ki,s}\boldsymbol{\rho}^e_i. \tag{45}$$

Although being nonzero, the last term on the right hand side of Eq. (45) can be omitted in the present setting, as it will never give a contribution to the proposed RSA design sensitivities. This is easily verified by reviewing the proposed RSA design sensitivities, using definition (19) and realizing that $\mathbf{B}^e\boldsymbol{\rho}^e_i = \mathbf{0}$. Evaluation of $\boldsymbol{\rho}^e_{i,s}$ involves partial derivatives of $\mathbf{q}^e_j$, $j = 1,\ldots,6$, which are given by

$$\begin{aligned} &\mathbf{q}^e_{i,s} = \mathbf{0}, && \boldsymbol{\omega}^e_{i,s} = \mathbf{0}, && i = 1,2,3,\\ &\mathbf{q}^e_{i+3,s} = \mathbf{e}_i \times \mathbf{x}_{0,s}, && \boldsymbol{\omega}^e_{i+3,s} = \mathbf{0}, && i = 1,2,3. \end{aligned} \tag{46}$$

In order to define $\boldsymbol{\rho}^e_{j,s}$, $j = 1,\ldots,6$ the exact definition of the nodal degrees of freedom has to be specified.

In Van Keulen and De Boer (1998a), details on the rigid body modes and their derivatives have been specified for a 12 degrees of freedom shell element (Van Keulen and Booij, 1996). As noted that formulation was restricted to linear analyses. With the foregoing results, extension to the nonlinear regime becomes straightforward.

5. Examples

Several numerical examples that study the effectiveness of the RSA method for different types of analyses will be presented. The well-known Koiter–Roorda frame (Koiter, 1967; Roorda, 1965) is considered in Section 5.1. RSA design sensitivities for both buckling and limit loads are compared with their traditional SA counterparts. For further comparison, global finite differences (GFD) will be used for buckling and nonlinear analyses. The present implementation of the GFD method for nonlinear analyses compensates for unbalance in the nonlinear solution (Haftka, 1993). Section 5.2 deals with sensitivities for linear, nonlinear and limit load analyses for a shallow shell roof as studied by Crisfield (1981) and Haftka (1993), among others. A deployable structure is subject of Section 5.3.

Results for the examples listed above are presented using logarithmic design sensitivities as functions of the relative design perturbation $\Delta s/s$. Logarithmic design sensitivities of a quantity α can be expressed as (Haftka, 1993)

$$\frac{\mathrm{d}(\log\alpha)}{\mathrm{d}(\log s)} = \frac{s}{\alpha}\,\frac{\mathrm{d}\alpha}{\mathrm{d}s}, \tag{47}$$

and have the advantage of being nondimensional and easy to interpret.

It was shown for the linear regime that RSA design sensitivities using forward finite differences are generally even more accurate than SA design sensitivities based on central finite differences. Moreover, the RSA alternative with forward finite differences is more efficient in terms of computer time as the mesh has to be perturbed only once. Therefore, central finite differences are not dealt with in the present article. A study concerning SA and RSA sensitivities using both forward and central finite differences for linear analyses can be found in Van Keulen and De Boer (1998a).

A widely used method to perturb a finite element mesh, is to perturb only elements that are located on a perturbed boundary. In case a surface description is used, *surface* coordinates of nodes at the interior are kept constant. Consequently, also elements at the interior of a surface get perturbed if the corresponding surface description is affected by a design variable. This approach is also adopted in the present work. The main advantage of this method is that often only a relatively small number of elements becomes perturbed. Hence, a reduction of the computational effort is achieved, as finite difference approximations of element matrices only have to be carried out for perturbed elements. A serious disadvantage concerns the relative perturbation $\Delta s/s$. This parameter is defined globally, which implies that the perturbation of a particular

element is not related to its dimensions. Thus, when refining the mesh, while keeping $\Delta s/s$ constant, the perturbation of elements relative to their dimensions will increase. Although the above is quite obvious, the reader should keep these considerations in mind when interpreting the numerical results presented in the next sections.

As a final remark, it is mentioned that a triangular finite rotation shell element is used for all numerical examples. A description of this element can be found in Van Keulen and Booij (1996).

5.1. Koiter–Roorda frame

A simple frame structure, as shown in Fig. 1, is considered. The length L of the two beams of the frame is chosen as the design variable. Buckling and post-buckling behaviour of this frame was studied analytically in Koiter (1967), where in particular the influence of imperfections on its post-buckling behaviour was investigated. Those analytical results are in excellent agreement with experimental observations reported in Roorda (1965). In the present article, the frame structure is modelled using shell elements with thickness t, with $t/L = 0.001$ in the nonperturbed configuration. The boundary conditions that have been used are depicted in Fig. 1. An imperfection in the loading condition has been introduced by a distributed moment m, with $m/pL \ll 1$. Due to membrane deformations in the pre-buckling solution, the finite element model without imperfection ($m = 0$) exhibits a limit point. This is in contrast with the analytical model (Koiter, 1967) where a bifurcation point occurs. On the basis of Koiter's (1967) result, the critical load parameter can be estimated by

$$\lambda_{\mathrm{cr}} = 1.1572\left(1 - 1.1514\sqrt{\frac{m}{pL}}\right)\frac{Et^3}{pL^2(1-\nu^2)}. \tag{48}$$

Notice that here the influence of membrane deformations on the pre-buckling solution are neglected. From differentiation of Eq. (48) to L, the logarithmic design sensitivity follows as

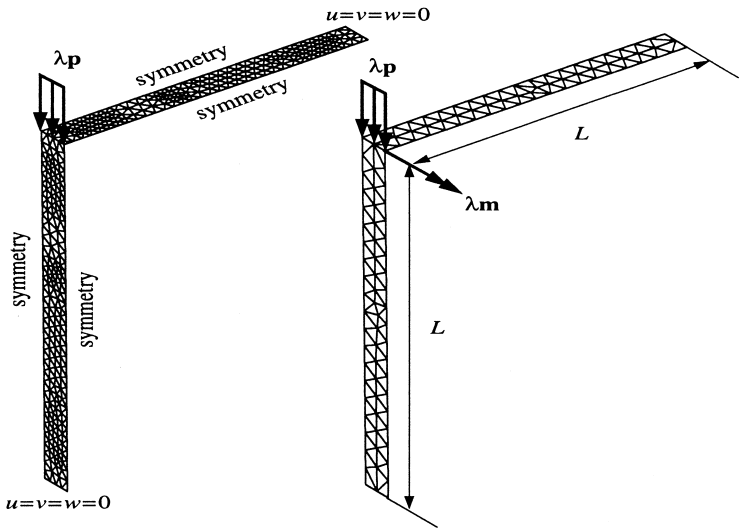

Fig. 1. Geometry and boundary conditions for a perfect frame and an imperfect one. The dimensions of the frame are characterized by $t/L = 0.001$, where t denotes the thickness. A load imperfection is introduced by a moment m about the connecting edge, with $m/pL = 0.001$. The applied load and the moment are scaled by a load parameter λ. A fine and a coarse mesh are used.

$$\frac{L}{\lambda_{\mathrm{cr}}}\frac{\mathrm{d}\lambda_{\mathrm{cr}}}{\mathrm{d}L}=\left(\frac{0.5757\sqrt{m/pL}}{1-1.1514\sqrt{m/pL}}\right)-2. \tag{49}$$

Herewith, it can be seen that the logarithmic design sensitivity of the critical load equals -2 for a perfect frame and -1.98 for the imperfect frame with $m/pL=0.001$.

Design sensitivities for the linearized buckling load of the perfect frame are given in Fig. 2. It is seen that the logarithmic derivative is approximately -2, which is in agreement with its analytical value. Furthermore, RSA design sensitivities are shown to be superior to SA design sensitivities and are nearly constant throughout the entire range of perturbations. As buckling loads are obtained by using a multi-vector iteration, application of the GFD method yields rather inaccurate results for smaller perturbations. Obviously, it is possible to improve the GFD results by requesting a higher accuracy in the multi-vector iteration (currently 10^{-3}), but this seriously increases the computer time needed.

Logarithmic design sensitivities for the critical load parameter are also investigated. Formally, these have to be evaluated *at* the limit point since only then $\mathbf{Jv}=\mathbf{0}$ holds true. In practice, it turns out to be sufficient to evaluate them rather close to the limit point. Corresponding results are presented in Fig. 3. At the same time, effects related to mesh refinement are examined. Fig. 3 shows that application of RSA sensitivities yields a tremendous improvement as compared to SA sensitivities. The difference even increases in favour of RSA sensitivities when refining the mesh, as their accuracy behaviour is not significantly affected by refinement of the mesh. The peak in the RSA sensitivities for the fine mesh and $\Delta L/L=10^{-3}$ can be explained by the fact that the relative perturbation $\Delta L/L$ is a global quantity. This means that if the mesh is refined, the relative perturbation of the smallest element may become rather large, although $\Delta L/L$ is kept constant. Furthermore, it is seen that the obtained results are in accordance with analytical results given by Eqs. (48) and (49).

Finally, the effects of imperfections on logarithmic design sensitivities for the critical load parameter are examined. Eq. (49) shows that the logarithmic design sensitivity for an imperfect frame is slightly less than the value for a perfect frame. This can also be observed from Fig. 4, where corresponding numerical results are presented. These results are obtained by making use of a coarse mesh, which is one of the reasons for the difference between numerical and analytical design sensitivities. Another reason might be the neglected influence of membrane deformations in the analytical results. From Fig. 4 it is seen that adding an imperfection does not noticeably influence the accuracy of RSA design sensitivities, whereas it does do so for SA design sensitivities. The reason for this is that deflections for an imperfect frame at critical load level will

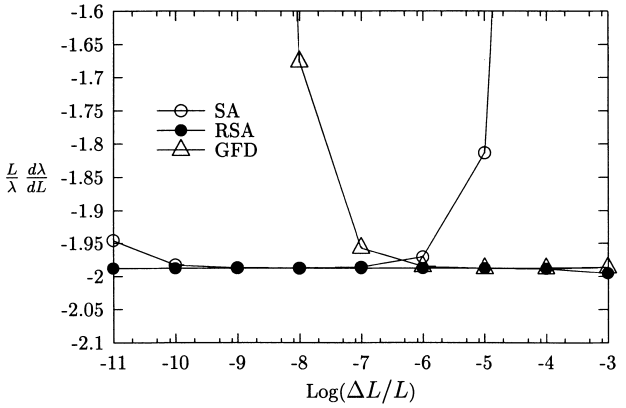

Fig. 2. Design sensitivities for the linearized buckling load of the perfect frame. The length L of the two beams of the frame is taken as the design variable and a coarse mesh is used. SA, RSA and GFD design sensitivities are compared.

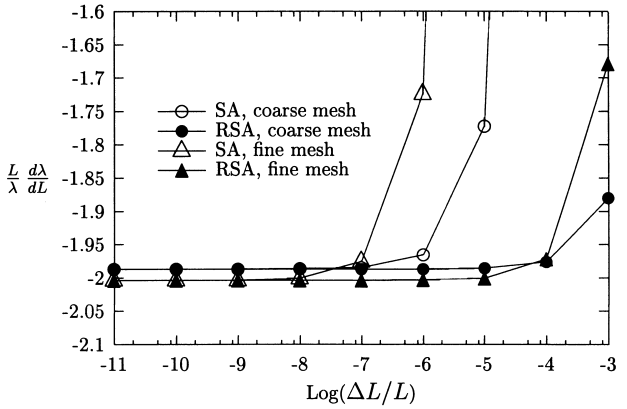

Fig. 3. Design sensitivities for the critical load parameter of the perfect frame. RSA and SA sensitivities are compared and the influence of mesh refinement is considered.

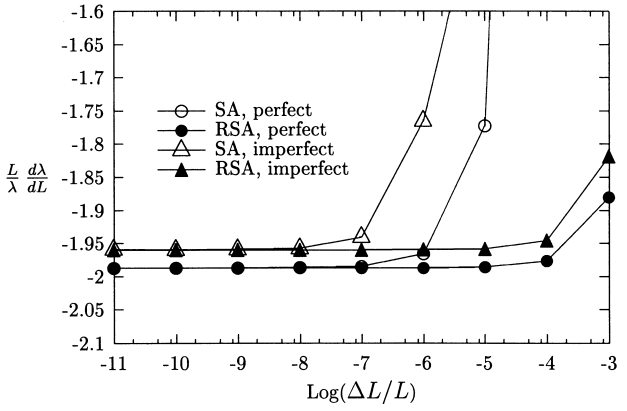

Fig. 4. Design sensitivities for the critical load parameter. A perfect and imperfect ($m/pL = 0.001$) frame are compared using a coarse mesh.

be much larger as compared to the perfect case, whereas the magnitude of the membrane deformations remains comparable. Hence, the ratio between rigid body motions and deformations increases.

5.2. Shallow shell roof

A hinged shallow cylindrical shell is examined (Crisfield, 1981; Haftka, 1993). Its geometry and boundary conditions are depicted in Fig. 5. The dimensions used are identical to those reported in Haftka (1993), i.e. $L = 252$ mm, $R = 2540$ mm and the thickness t equals 6.35 mm. The material properties are specified as $E = 3105$ N/mm^2 and $v = 0.3$. The critical load for a symmetric deformation pattern was found to be 575.6 N. Due to symmetry, only a quarter of the roof is analysed. In this sub-section, the design sensitivities with respect to the radius R are considered. Note, that L is kept constant. In Haftka (1993), design sensitivities for the sizing variables t and v were examined. Although not reported here, these sensitivities were also investigated and appeared to be in agreement with those given in Haftka (1993).

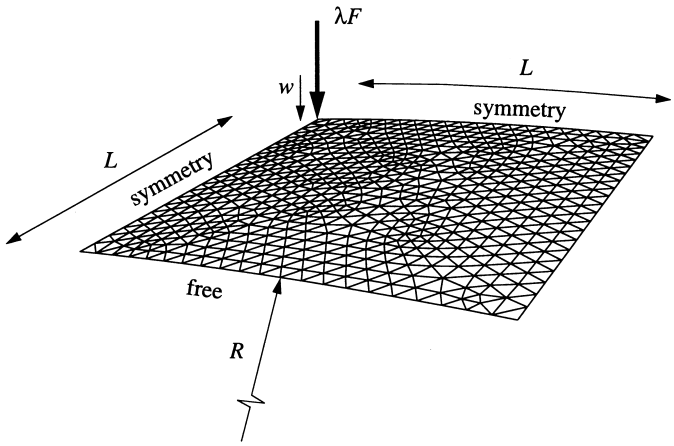

Fig. 5. Geometry of shallow shell roof. Dimensions are $L = 252$ mm, $R = 2540$ mm and $F = 0.25$ N. Thickness t equals 6.35 mm.

Fig. 6 presents design sensitivities for the vertical displacement w at the centre of the roof. The results correspond to a linear analysis using the mesh shown in Fig. 5. SA, RSA and GFD design sensitivities are explored. It is observed that the accuracy of RSA design sensitivities is as good as that of GFD design sensitivities. However, SA design sensitivities are rather inaccurate for larger design perturbations.

The design sensitivities for a nonlinear analysis are depicted in Fig. 7. These are computed at $\lambda = 500$, i.e. at about 85% of the critical load. Again, results of the RSA method are in close accordance with those of the GFD approach and are almost constant throughout the whole range of perturbations. Note the difference between the logarithmic design sensitivity for the linear case and the nonlinear one.

Attention is also paid to design sensitivities for the critical load. The same remark as given in Section 5.1 about computing design sensitivities according to Eq. (31) holds true. Fig. 8 shows that application of the RSA method yields the better results, i.e. they depend less on the choice of the relative design perturbation $\Delta s/s$.

The results for the shallow shell roof clearly address the supremacy of RSA over SA design sensitivities.

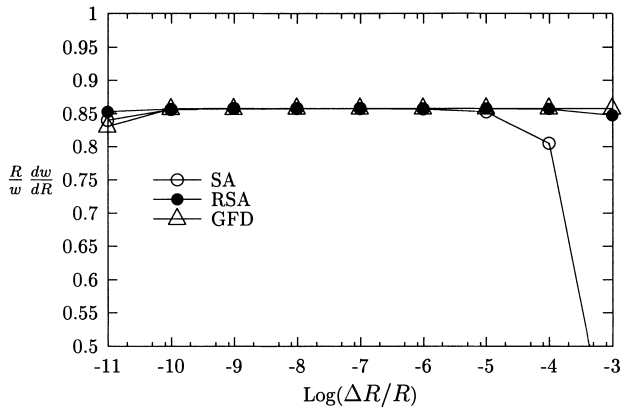

Fig. 6. Design sensitivity for vertical displacement w at the centre corresponding to a linear analysis.

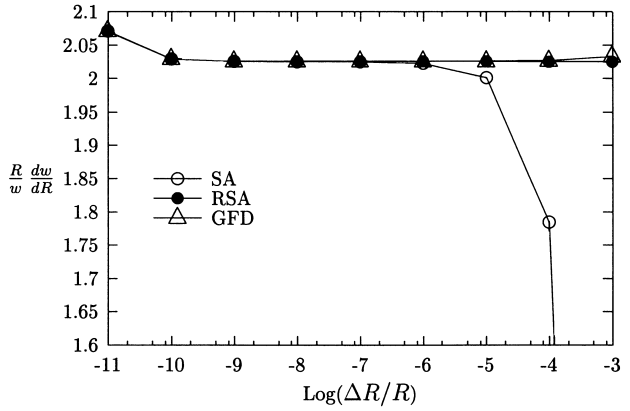

Fig. 7. Design sensitivity for vertical displacement w at the centre for $\lambda = 500$.

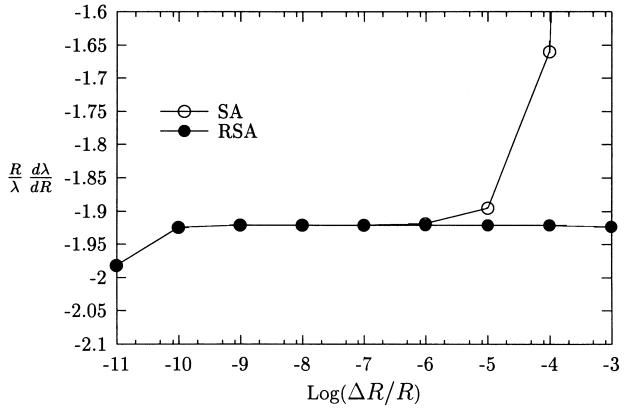

Fig. 8. Design sensitivities for the critical load of the shallow shell roof.

5.3. Petal

During folding and unfolding, deployable structures often undergo large displacements and finite rotations, whereas the deformations remain relatively small. Refined SA design sensitivities are therefore expected to be especially useful for these type of structures. The present sub-section investigates a deployable structure, namely a petal which is fully clamped at the circular hub. Eight of such petals in the deployed configuration form a spherical cap, with a radius R. It holds that $R/r = 5.9$, where r denotes the radius of the hub. The thickness of the petal is specified by t, and $R/t = 100$. The material properties are given as $E = 2.10^5$ N/mm^2 and $v = 0.3$. The geometry and boundary conditions of the petal are presented in Fig. 9. Both free sides of the petal are described by using the description for an ordinary line, but in terms of spherical coordinates. The petal is loaded by a unit distributed bending moment m, which is scaled by a load parameter λ. The location of point A is controlled by the design variable ϕ. Design sensitivities for the displacement component in x-direction of point A are considered in the folded configuration, which is reached at $\lambda = 0.45$.

The design sensitivities for a nonlinear analysis are presented in Fig. 10. Again, the results corresponding to the RSA method are nearly constant throughout the complete range of relative design perturbations. On

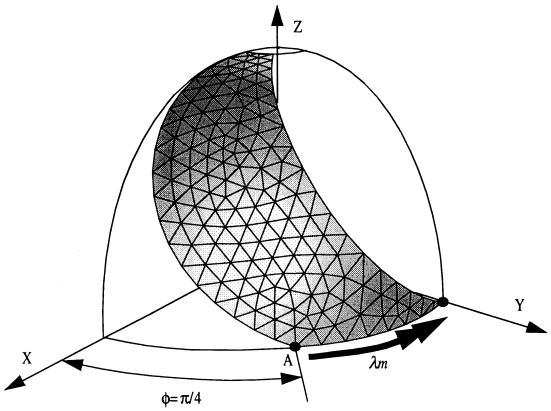

Fig. 9. Geometry and boundary conditions of the deployed petal. The angle ϕ is chosen as the design variable.

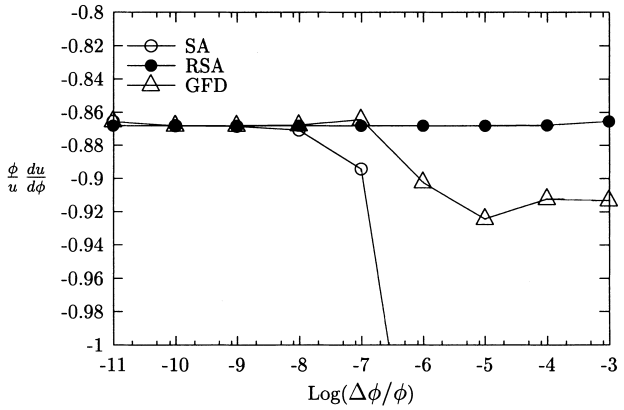

Fig. 10. Design sensitivities for the displacement of point A in the x direction in the folded configuration. SA, RSA and GFD design sensitivities are explored.

the contrary, SA design sensitivities behave in an extremely undesired manner, which is caused by the nature of the problem. Folding of the petal can be considered as a problem exhibiting almost inextensional bending. Hence, the RSA approach takes full advantage of the analytical differentiation of rigid body motions at the element level.

6. Discussion and conclusions

Refined semi-analytical design sensitivities have been constructed using rigid body modes of individual elements and their analytical derivatives. In contrast to previous papers, here a sound and unified formulation is given for nonlinear, linear, limit-point and linearized buckling analyses. The starting point is a decomposition of the contribution to the pseudo-load vector associated to internal stresses. Apart from being a fundamental step towards improved semi-analytical design sensitivities, this decomposition also provides a better understanding of the actual nature of errors introduced by finite difference approximations used for evaluation of the pseudo-load vector. After this decomposition has been accomplished,

consistency conditions permit elimination of certain partial derivatives, normally approximated by finite differences. This can be done by virtue of analytical derivatives of the rigid body modes that have been made available. Finally, in the case of a linear or a linearized buckling analysis, a decomposition of the displacement field or the buckling mode is carried out, respectively. Again, consistency equations permit elimination of specific partial derivatives. For linearized buckling analyses, a decomposition of the pseudo-load vector is not required.

Implementation of the proposed refinements is easy, especially if compared to analytical derivatives. The basis for an RSA implementation is identical to a standard SA implementation. A part of the additional implementation task can be done generically. From the formulation it also becomes apparent, that the additional effort in terms of computing times is very small. As an example, the RSA formulation for geometrically nonlinear analyses is considered. The differences between the SA and the RSA formulation are reflected by Eqs. (24) and (26). Comparing these equations, it is seen that the contribution $\mathbf{B}_{,s}^{e\mathrm{T}}\boldsymbol{\sigma}^{e}$ has to be multiplied by both $\mathbf{S}^{e}$ and $\mathbf{F}^{e}$ in the refined formulation. Moreover, these matrices have to be generated using information on rigid body modes and their derivatives. Consequently, it is concluded that the required additional computing effort is negligible.

Numerical results corresponding to an RSA formulation are generally superior to results based on an SA formulation. It is noted that the proposed refinements are fully compatible with more advanced design perturbation schemes and can be combined with improved finite difference schemes. As an example, the method can be combined with higher-order finite difference schemes without any complication.

In the present article design sensitivities for geometrically nonlinear analyses have been discussed under the assumption of a load parameter which is independent of the design variables and which is prescribed. Without any difficulties, it is possible to adopt the RSA strategy for other types of geometrically nonlinear analyses, for example, on the basis of arc-length control.

Obviously, if analytical derivatives of the FE matrices are available, e.g. due to the application of automated differentiation techniques, these exact formulations should be preferred above approximations on the basis of finite differences.

Finally, it is recommended to give preference to an RSA formulation over an SA formulation at all times, as the results obtained are just as good or much better, while the additional costs for implementation and computing are minor.

Acknowledgements

The authors wish to acknowledge the comments and suggestions on the manuscript made by Prof. R.T. Haftka (University of Florida).

References

Argyris, J., Mlejnek, H.P., 1986. Die Methode der Finiten Elemente, vol. I: Verschiebungsmethode in der Statik. Braunschweig, Vieweg.

Barthelemy, B., Haftka, R.T., 1988. Accuracy analysis of the semi-analytical method for shape sensitivity calculation. Proc. AIAA/ASME/ASCE/ASC 29th Structures, Structural Dynamics and Materials Conf., Williamsburg, VA. AIAA paper 88–2284.

Barthelemy, B., Chon, C.T., Haftka, R.T., 1988. Accuracy problems associated with semi-analytical derivatives of static response. Finite Elem. Anal. and Design 4, 249–265.

Cheng, G., Gu, Y., Zhou, Y., 1989. Accuracy of semi-analytic sensitivity analysis. Finite Elem. Anal. and Design 6, 113–128.

Cheng, G., Olhoff, N., 1993. Rigid body motion test against error in semi-analytical sensitivity analysis. Struct. Optimiz. 46, 515–527.

Crisfield, M.A., 1981. A fast incremental/iterative solution procedure that handles "snap-through". Comp. and Struct. 13, 55–62.

De Boer, H., Van Keulen, F., 1997a. Error analysis of refined semi-analytical design sensitivities. Struct. Optimiz. 14, 242–247.

De Boer, H., Van Keulen, F., 1997b. Improved semi-analytic design sensitivities for a linear and finite rotation shell element. In: Gutkowski, W., Mróz, Z. (Eds.), WCSMO-2, Second World Congress of Structural and Multidisciplinary Optimization. pp. 199–204.

Fenyes, P., Lust, R.V., 1991. Error analysis of semianalytic displacement derivatives for shape and sizing variables. AIAA Journal 29, 271–279.

Haftka, R.T., Adelman, H.M., 1989. Recent developments in structural sensitivity analysis. Struct. Optimiz. 1, 137–151.

Haftka, R.T., Gürdal, Z., 1992. Elements of Structural Optimization. Third ed. Kluwer Academic Publishers, Dordrecht, Netherlands.

Haftka, R.T., 1993. Semi-analytical static nonlinear structural sensitivity analysis. AIAA Journal 31 (7), 1307–1312.

Hinton, E., Sienz, J., Afonso, S.M.B., 1995. Experiences with Olhoff's "exact" semi-analytical sensitivity algorithm. In: Olhoff, N., Rozvany, G.I.N. (Eds.), WCSMO-1, First World Congress of Structural and Multidisciplinary Optimization, Pergamon, New York, NY, pp. 41–46.

Kleiber, M., Hien, T.D., 1997. Parameter sensitivity of inelastic buckling and post-buckling response. Comput. Meth. Appl. Mech. Engng. 145, 239–262.

Koiter, W.T., 1967. Post-buckling analysis of a simple two-bar frame', In: Broberg, B., Hult, J., Niordson, F. (Eds.), Recent Progress in Applied Mechanics, The Folke Odqvist, vol. B, Almqvist & Wiksell, Stockholm.

Lund, E., Olhoff, N., 1994. Shape design sensitivity analysis of eigenvalues using "exact" numerical differentiation of finite element matrices. Struct. Optimiz. 8, 52–59.

Mlejnek, H.P., 1992. Accuracy of semi-analytical sensitivities and its improvement by the "natural method". Struct. Optimiz. 4, 128–131.

Mróz, Z., Haftka, R.T., 1994. Design sensitivity analysis of non-linear structures in regular and critical states. Int. J. Solids Struct. 31 (15), 2071–2098.

Olhoff, N., Rasmussen, J., 1991. Study of inaccuracy in semi-analytical sensitivity analysis – a model problem. Struct. Optimiz. 3, 203–213.

Olhoff, N., Rasmussen, J., Lund, E., 1993. A method of "exact" numerical differentiation for error elimination in finite-element-based semi-analytical shape sensitivity analyses. Mech. Struct. Mach. 21, 1–66.

Pedersen, P., Cheng, G., Rasmussen, J., 1989. On accuracy problems for semi-analytical sensitivity analyses. Mech. Struct. Mach. 17, 373–384.

Riks, E., 1997. Buckling analysis of elastic structures: A computational approach. Adv. Appl. Mech. 34, 1–76.

Roorda, J., 1965. Stability of structures with small imperfections, J. Engng. Mech. Div. ASCE 91, EM 1, Proc. Paper 4230, 87.

Seyranian, A.P., Lund, E., Olhoff, N., 1994. Multiple eigenvalues in structural optimization problems. Struct. Optimiz. 8, 207–227.

Keulen, F., Booij, J., 1996. Refined consistent formulation of a curved triangular finite rotation shell element. Int. J. Num. Meth. Engng. 39, 2803–2830.

Keulen, F., De Boer, H., 1998a. Rigorous improvement of semi-analytical design sensitivities by exact differentiation of rigid body motions. Int. J. Numer. Meth. Engng. 42, 71–91.

Van Keulen, F., De Boer, H., 1998b. Refined semi-analytical design sensitivities for buckling. In: Seventh AIAA/USAF/NASA/ISSMO Symposium on Multidisciplinary Analysis and Optimization, St. Louis, Missouri, part 1, AIAA-98-4761, pp. 420–429.

Wu, C.C., Arora, J.S., 1987. Design sensitivity analysis and optimization of nonlinear structural response using incremental procedure. AIAA Journal 25 (8), 1118–1125.

Wu, C.C., Arora, J.S., 1988. Design sensitivity analysis of non-linear buckling load. Comput. Mech, 3,129–140.